Improved High-Frequency Voltage Injection Based Permanent Magnet Temperature Estimation for PMSM Condition Monitoring for EV Applications

Guodong Feng, *Member, IEEE*, Chunyan Lai, *Member, IEEE*, K. Lakshmi V. Iyer, *Member, IEEE*, and Narayan C. Kar, *Senior Member, IEEE*

***Abstract*—Permanent magnet (PM) temperature is critical to ensure high-performance and reliable control of permanent magnet synchronous machines (PMSMs) for electric vehicle (EV) applications. High-frequency (HF) voltage injection based approach has been shown to be capable of PM temperature estimation under all-speed range with simple implementation. This paper improves existing HF voltage injection based PM temperature estimation approach by considering the cross-coupling effect. The key to PM temperature estimation is the temperature-dependent HF resistance estimated from the injected HF voltage and the current response. It is found that the cross-coupling effect has a great influence on the HF resistance estimation. This paper firstly improves the HF voltage injection model by considering the cross-coupling effect. Then, a comparative numerical investigation is conducted to analyze the estimation errors induced by the cross-coupling effect. A novel HF resistance estimation approach is derived from the proposed improved model and the PM temperature is calculated from the HF resistance with a linear thermal model. The influence of inverter nonlinearity is also analyzed. Experimental investigations demonstrate that the proposed approach is able to improve the performance of PM temperature estimation.**

***Index Terms*—Condition monitoring, cross-coupling effect, EV, HF voltage injection, mutual inductance, PM temperature.**

I. Introduction

PERMANENT magnet synchronous machines (PMSMs) have been widely used in automotive applications due to their high power density, high efficiency and fast dynamic performance [1]–[4]. High-performance and reliable PMSM drives are of significance in electric vehicle (EV) applications. Permanent magnet (PM) temperature is a critical parameter to achieve high-performance and reliable control of PMSMs. This is due to high current requirement of PMSMs to deliver the propulsion torque in EV applications, thus the issue of temperature rise is inevitable. Some machine parameters such as magnet flux linkage are temperature-dependent [5]–[7], and therefore accurate PM temperature can help to compensate parameter variations to improve the PMSM drive performance. Moreover, excessive temperature could cause permanent demagnetization of PMs. Thus, the temperature information can be used to monitor the PM condition to avoid damage to the machine.

The winding temperature can be accurately measured by using the contact-type sensors. However, direct measure of PM temperature is a challenging task [8]. Techniques like infrared imaging and thermal detectors have difficulties in installation and raise cost concerns. Therefore, PM temperature estimation has aroused considerable interests. In the literature, there are mainly two kinds of PM temperature estimation approaches. One is thermal network based approach and the other is the machine model based approach. Thermal network based approach employs the thermal network to model the heat transfer in the machine [9], which requires accurate knowledge of the machine geometric structure that is not always available and thus has limited applicability. The machine model based approach employs available sensor measurements to estimate the PM temperature-dependent machine parameters. It can be further divided into the high-frequency (HF) signal injection approach that estimates the temperature-dependent HF resistance and the fundamental approach that estimates the temperature-dependent rotor flux [10]–[13]. In particular, this paper focuses on HF signal injection based approach due to its a good estimation performance in all-speed range.

HF signal injection based approach has been widely studied in the literature [14]–[17]. In this approach, a carrier signal whose frequency is much higher than the fundamental frequency is injected into the machine to generate an HF signal response for HF resistance estimation, and the PM temperature is estimated from the HF resistance using a linear thermal model. In general, the carrier signal can be either an HF voltage or an HF current signal. In the HF voltage injection based approach [18], an HF voltage signal is injected into the machine and the HF resistance is estimated from the HF current response. In the HF current injection based approach [19], [20], an HF current signal is injected into the machine and the HF resistance is estimated from the HF voltage response. The HF current injection requires an additional current controller, and an improper design of the current controller will deteriorate its PM temperature estimation performance. However, the HF voltage injection has a simple implementation as the HF voltage can be directly added to the

Manuscript received March 15, 2017; revised August 29, 2017 and October 21, 2017; accepted November 6, 2017. Date of publication November 29, 2017; date of current version January 15, 2018. The review of this paper was coordinated by the Guest Editors of the VPPC 2016 Special Section. *(Corresponding author: Guodong Feng.)*

The authors are with the Department of Electrical and Computer Engineering, University of Windsor, Windsor, ON N9B 3P4, Canada (e-mail: guodong.feng@uwindsor.ca; lai112@uwindsor.ca; iyerl@uwindsor.ca; nkar@uwindsor.ca).

Color versions of one or more of the figures in this paper are available online at http://ieeexplore.ieee.org.

Digital Object Identifier 10.1109/TVT.2017.2778429

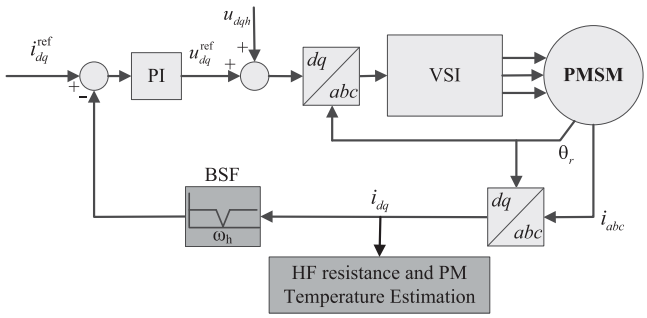

Fig. 1. The control diagram with HF voltage injection, where variables with superscript 'ref' denote the reference values, u_{dqh} is the injected HF signal, BSF means band stop filter, and VSI means voltage source inverter.

stator reference voltages. Thus, this paper considers HF voltage injection for PM temperature estimation.

The cross-coupling effect has been neglected in existing studies during PM temperature estimation. Recent studies [21]–[25] show that cross-coupling effect has a great influence on the performance of HF voltage injection for sensorless control. This paper will demonstrate that the cross-coupling effect has great influence on the HF resistance estimation as well, and neglecting this effect will cause great error in the PM temperature estimation.

This paper improves the HF voltage injection based PM temperature estimation by considering the cross-coupling effect. Firstly, the HF voltage injection model for HF resistance estimation considering cross-coupling effect is developed and validated. Extensive numerical studies have been performed to demonstrate how cross-coupling effect affects the HF resistance estimation. Then, a novel approach based on this model is developed for HF resistance estimation. The inverter nonlinearity will affect the HF voltage injection and thus the HF resistance estimation [25]. Hence, an analysis on inverter nonlinearity is proposed. The proposed approach is validated with experiments on a laboratory PMSM drive system.

II. PM Temperature Estimation Using HF Resistance

This paper employs the HF voltage injection for HF resistance estimation. As shown in Fig. 1, when an HF voltage is superimposed on the dq-axis voltages, an HF current response will be induced in the dq-axis currents and the HF resistance can be estimated from the HF components, which will be detailed in next section.

According to [18], [19], the HF resistance consists of the stator and rotor HF resistances. The HF resistance increases linearly with the increase of PM temperature. Therefore, the PM temperature can be estimated from the HF resistance with a linear thermal model. It should be noted that the capacitance effect is neglected in this paper because the frequency of the injected signal is in the range of a few hundred Hertz, in which the capacitance effect is negligible [30], [31]. On the other hand, this paper mainly focuses on improving the estimation performance by considering cross-coupling effect. Compared with the capacitance effect, the cross-coupling effect has a more significant impact on the estimation performance. Inclusion of the capacitance effect can further improve the estimation performance, but it is beyond the scope of this paper and can be explored in future work.

Without loss of generality, this paper considers using d-axis HF resistance for PM temperature estimation. It should be noted that q-axis HF resistance can also be used, but it is suggested to use the d-axis HF resistance for temperature estimation. This is because q-axis HF current will produce high torque ripples that may affect the drive performance.

Let R_{dh} denotes the d-axis HF resistance. According to [17]–[19], R_{dh} consists of two parts: one is the stator contributed HF resistance and the other is the rotor contributed HF resistance. Therefore, R_{dh} can be denoted as

$$R_{dh} = R_{dh}^{s} + R_{dh}^{r} \tag{1}$$

where R_{dh}^{s} and R_{dh}^{r} are the stator and rotor contributed HF resistances, respectively. Here, R_{dh}^{s} is winding temperature dependent and R_{dh}^{r} is PM temperature dependent [18], [19]. The relationships between temperature and HF resistance are

$$\begin{aligned} R_{dh}^{s} &= R_{dhT_0}^{s}\left[1+\alpha_{cu}(T_W - T_0)\right] \\ R_{dh}^{r} &= R_{dhT_0}^{r}\left[1+\alpha_{mag}(T_{PM} - T_0)\right] \end{aligned} \tag{2}$$

where α_{cu} and α_{mag} are the copper and magnet thermal resistive coefficients; $R_{dhT_0}^{s}$ and $R_{dhT_0}^{r}$ are the stator and rotor HF resistances at T_0; T_W and T_{PM} are the stator winding and rotor PM temperatures. Both R_{dh}^{s} and R_{dh}^{r} increase with the rise of temperature. Based on (1) and (2), the PM temperature can be computed from

$$T_{PM} = T_0 + \frac{R_{dh} - R_{dh}^{s} - R_{dhT_0}^{r}}{R_{dhT_0}^{r}\alpha_{mag}} \tag{3}$$

From (3), the estimation of PM temperature requires the prior knowledge of the stator and rotor HF resistance at room temperature, $R_{dhT_0}^{s}$ and $R_{dhT_0}^{r}$, and the winding temperature T_W. $R_{dhT_0}^{s}$ and $R_{dhT_0}^{r}$ can be obtained at machine commissioning and T_W can be obtained with a thermal detector which is available in existing PMSMs for EV applications. Thus, the key to PM temperature estimation is the HF resistance.

III. HF Resistance Estimation Considering Cross-Coupling Effect

This section firstly improves the existing HF voltage injection model by considering cross-coupling effect, and then derives the HF resistance estimation approach and analyzes the influence of inverter nonlinearity and PM flux variation on the HF resistance estimation.

A. Existing HF Voltage Injection Model

The dq-axis PMSM model can be represented as

$$\begin{bmatrix} u_d \\ u_q \end{bmatrix} = \begin{bmatrix} R_d + pL_d & -\omega L_q \\ \omega L_d & R_q + pL_q \end{bmatrix} \begin{bmatrix} i_d \\ i_q \end{bmatrix} + \omega \begin{bmatrix} 0 \\ \lambda_M \end{bmatrix} \tag{4}$$

where u_d, u_q and i_d, i_q are the dq-axis voltages and currents, respectively, R_d, R_q and L_d, L_q are the dq-axis resistances and

inductances, respectively, ω is the rotor speed, λ_M is the PM flux, p is the differential operator.

When an HF voltage signal is injected into the machine, the HF model can be denoted as (5) [18].

$$\begin{bmatrix} u_{dh} \\ u_{qh} \end{bmatrix} = \begin{bmatrix} R_{dh} + j\omega_h L_{dh} & 0 \\ 0 & R_{qh} + j\omega_h L_{qh} \end{bmatrix} \begin{bmatrix} i_{dh} \\ i_{qh} \end{bmatrix} \quad (5)$$

where the differential operation p is replaced by $j\omega_h$, and ω_h is the angular frequency of the HF signal. Here, the subscript "h" in (5) represents the HF components or HF machine parameters, which hold through this paper. It should be emphasized that the high-pass filter mentioned is to demonstrate the concept that the HF component can be segregated, and thus the HF model can be represented in the form of (5). However, the high-pass filter is not required for HF component extraction.

In existing approaches, the HF resistance is estimated from the HF voltage and the induced HF current response based on the model (5), in which the cross-coupling effect is neglected.

B. Improved HF Voltage Injection Model

When the cross-coupling effect is considered, the dq-axis PMSM model can be represented as in (6) [24].

$$\begin{bmatrix} u_d \\ u_q \end{bmatrix} = \begin{bmatrix} R_d + pL_d & -\omega L_q + pL_{dq} \\ \omega L_d + pL_{qd} & R_q + pL_q \end{bmatrix} \begin{bmatrix} i_d \\ i_q \end{bmatrix} + \omega \begin{bmatrix} 0 \\ \lambda_M \end{bmatrix} \quad (6)$$

where the definition of parameters is the same as that in (4). Here, L_{dq} and L_{qd} are the dq-axis mutual inductances that model the cross-coupling between the d and q axis. The mutual inductances are assumed to be equal, that is,

$$L_{dq} = L_{qd} \quad (7)$$

When an HF voltage signal is injected into the machine, the improved HF model considering cross-coupling effect is

$$\begin{bmatrix} u_{dh} \\ u_{qh} \end{bmatrix} = \begin{bmatrix} R_{dh} + j\omega_h L_{dh} & j\omega_h L_{dq} - \omega L_{qh} \\ j\omega_h L_{qd} + \omega L_{dh} & R_{qh} + j\omega_h L_{qh} \end{bmatrix} \begin{bmatrix} i_{dh} \\ i_{qh} \end{bmatrix} \quad (8)$$

where L_{dh} and L_{qh} are the dq-axis self-inductances. Compared with existing model (5), the main differences in the proposed model (8) are i) the mutual inductance terms are considered; and ii) the terms $-\omega L_{qh} i_{qh}$ and $\omega L_{dh} i_{dh}$ are considered.

C. Proposed HF Resistance Estimation Approach

When an HF voltage in (9) is injected into the machine, the d-axis HF current response is shown in (10).

$$\begin{bmatrix} u_{dh} & u_{qh} \end{bmatrix}^T = \begin{bmatrix} V_{dh} \cos\omega_h t & 0 \end{bmatrix}^T \quad (9)$$

$$i_{dh} = \frac{u_{dh}}{(R_{dh} + j\omega_h L_{dh}) + \frac{(\omega L_{dh} + j\omega_h L_{qd})(\omega L_{qh} - j\omega_h L_{dq})}{R_{qh} + j\omega_h L_{qh}}} \quad (10)$$

where V_{dh} is the magnitude of the injected HF voltage and ω_h is the frequency. It can be seen from (10) that the d-axis HF current response contains additional terms induced by cross-coupling effect. According to (10), the d-axis HF impendence can be represented in the form of

$$Z_{dh} = R_{dh} + j\omega_h L_{dh} + \frac{(\omega L_{dh} + j\omega_h L_{qd})(\omega L_{qh} - j\omega_h L_{dq})}{R_{qh} + j\omega_h L_{qh}} \quad (11)$$

The HF voltage and its current response, u_{dh} and i_{dh}, can be obtained from the measurements, thus d-axis HF impendence can be estimated from these current and voltage measurements. To this end, the d-axis HF current i_{dh} in (10) is reformulated as in (12) and the estimated d-axis HF impedance $\hat{Z}_{dh}$ is represented as in (13).

$$i_{dh} = I_{dh} \cos(\omega_h t - \phi_{Zdh}) \quad (12)$$

$$\hat{Z}_{dh} = \hat{R}_{dh} + j\omega_h \hat{L}_{dh} \quad (13)$$

where I_{dh} and ϕ_{Zdh} are the magnitude and phase angle of i_{dh}, respectively, and they can be extracted from d-axis current, which will be detailed in Section IV. Here, the variable with "$\hat{}$" denotes that it is estimated from the measurements.

After the magnitude and phase angle of u_{dh} and i_{dh} are extracted from the corresponding measurements, the d-axis HF resistance and inductance can be estimated from

$$|\hat{Z}_{dh}| = V_{dh}/I_{dh} \quad (14)$$

$$\hat{R}_{dh} = |\hat{Z}_{dh}| \cos\phi_{Zdh} \quad (15)$$

$$\omega_h \hat{L}_{dh} = |\hat{Z}_{dh}| \sin\phi_{Zdh} \quad (16)$$

Comparing (11) with (13), it can be found that the estimated impedance is unequal to the actual one due to cross-coupling effect. When this effect is considered, the relationship between the estimated d-axis HF impedance and the actual one is derived in (17) using (11) and (13).

$$\hat{R}_{dh} + j\omega_h \hat{L}_{dh} = R_{dh} + j\omega_h L_{dh} + \frac{(\omega L_{dh} + j\omega_h L_{qd})(\omega L_{qh} - j\omega_h L_{dq})}{R_{qh} + j\omega_h L_{qh}} \quad (17)$$

Based on (17), the relationship between the actual R_{dh}, L_{dh} and the estimated $\hat{R}_{dh}$, $\hat{L}_{dh}$ are

$$\hat{R}_{dh} = R_{dh} + (k_1^2 k_2 + k_3^2) R_{qh} + k_1 k_4 (1 - k_2) \omega_h L_{dh} \quad (18)$$

$$\hat{L}_{dh} = (1 - k_1^2 - k_3 k_4) L_{dh} + k_1 k_3 (1 - k_2) R_{qh}/\omega_h \quad (19)$$

where

$$k_1 = \tfrac{\omega}{\omega_h},\ k_2 = \tfrac{L_{dh}}{L_{qh}},\ k_3 = \tfrac{L_{dq}}{L_{qh}},\ k_4 = \tfrac{L_{dq}}{L_{dh}} \quad (20)$$

Proof: see Appendix. ■

The last term in (19) is much smaller than the actual inductance L_{dh}. For instance, when $\omega = 80\,\pi$ rad/s and $\omega_h = 500\,\pi$ rad/s, the last term is $3.1e^{-3}$ mH, which can be neglected. Hence, (18) and (19) can be simplified as in (21) and (22).

$$\hat{R}_{dh} = R_{dh} + (k_1^2 k_2 + k_3^2) R_{qh} + k_1 k_4 (1 - k_2) \omega_h L_{dh} \quad (21)$$

$$\hat{L}_{dh} = (1 - k_1^2 - k_3 k_4) L_{dh} \quad (22)$$

From (21) and (22), when ω_h is high enough, the estimated $\hat{R}_{dh}$ is larger than the actual R_{dh} and the estimated $\hat{L}_{dh}$ is smaller than the actual L_{dh} due to cross-coupling effect.

After $\hat{R}_{dh}$ and $\hat{L}_{dh}$ are estimated from (15) and (16), the actual R_{dh} can be obtained from (23) according to (21).

$$R_{dh} = \hat{R}_{dh} - (k_1^2 k_2 + k_3^2) R_{qh} - \frac{k_1 k_4 (1 - k_2)}{1 - k_1^2 - k_3 k_4} \omega_h \hat{L}_{dh} \tag{23}$$

For the test machine, it is assumed that R_{dh} is equal to R_{qh}. From this, (23) can be simplified as

$$R_{dh} = \frac{1}{1 + k_1^2 k_2 + k_3^2} (\hat{R}_{dh} - \frac{k_1 k_4 (1 - k_2)}{1 - k_1^2 - k_3 k_4} \omega_h \hat{L}_{dh}) \tag{24}$$

It can be seen from (24) that the actual d-axis HF resistance, R_{dh}, can be estimated from the linear combination of the estimated HF resistance $\hat{R}_{dh}$ and the estimated HF inductance $\hat{L}_{dh}$. Moreover, the HF resistance estimation requires the mutual and HF inductances of the machine. From (22), the coefficient $1 - k_1^2 - k_3 k_4$ is close to 1. For instance, when ω_h is selected to be 10 times larger than ω and L_{dq} is less than 10% of the dq-axis HF inductance, we have $1 - k_1^2 - k_3 k_4 > 0.98$. Therefore, based on (22), we can assume that

$$\hat{L}_{dh} \approx L_{dh} \tag{25}$$

It should be noted that this approximation in (25) will be used only for calculating the coefficients $k_1, \ldots, k_4$.

The q-axis HF resistance and inductance can be estimated following above d-axis HF inductance estimation. Specifically, when an HF voltage signal (26) is injected into the machine, the induced q-axis HF current response can be denoted as (27).

$$\begin{bmatrix} u_{dh} & u_{qh} \end{bmatrix}^T = \begin{bmatrix} 0 & V_{qh} \cos \omega_h t \end{bmatrix}^T \tag{26}$$

$$i_{qh} = I_{qh} \cos(\omega_h t - \phi_{Zqh}) \tag{27}$$

where V_{qh} is the magnitude of the injected HF voltage and ω_h is the frequency, I_{qh} and ϕ_{Zqh} are the magnitude and the phase angle of i_{qh}, respectively. Similar as (14)–(19), the q-axis HF resistance and inductance can be estimated from

$$\hat{Z}_{qh} = \hat{R}_{qh} + j \omega_h \hat{L}_{qh} \tag{28}$$

$$|\hat{Z}_{qh}| = V_{qh} / I_{qh} \tag{29}$$

$$\hat{R}_{qh} = |\hat{Z}_{qh}| \cos \phi_{Zqh} \tag{30}$$

$$\omega_h \hat{L}_{qh} = |\hat{Z}_{qh}| \sin \phi_{Zqh} \tag{31}$$

$$\hat{R}_{qh} = R_{qh} + (k_1^2 / k_2 + k_4^2) R_{dh} + k_1 k_4 (1 - k_2) \omega_h L_{qh} \tag{32}$$

$$\hat{L}_{qh} = (1 - k_1^2 - k_3 k_4) L_{qh} \tag{33}$$

From the analysis of (25), (33) can be approximately written as (34), which will be used only for calculating $k_1, \ldots, k_4$.

$$\hat{L}_{qh} \approx L_{qh} \tag{34}$$

In order to estimate the HF resistance using (23), the coefficients k_1, k_2, k_3 and k_4 should be known, which requires the information of dq-axis HF inductances and mutual inductance. Therefore, offline tests are necessary to obtain the parameters for HF resistance estimation. Specifically, the dq-axis HF inductances can be approximated by using (25) and (34), and the mutual inductance can be estimated by using existing approaches [23], [24], [22], [27].

Algorithm 1: *R_{dh} Estimation.*

1: Inject HF signal (9) when the motor speed is stable
2: Detect the HF components from the measurements
3: Use (15) and (16) to calculate $\hat{R}_{dh}$ and $\hat{L}_{dh}$
4: Use (24) to calculate R_{dh}

Three approximations have been made including $\hat{L}_{dh} \approx L_{dh}$, $\hat{L}_{qh} \approx L_{qh}$ and $R_{dh} \approx R_{qh}$ in HF resistance estimation. Therefore, it is necessary to investigate how these approximations influence the accuracy of HF resistance estimation. From (23), the estimation error due to these approximations is

$$\begin{aligned} R_{dh}^{err} = {} & (k_1^2 k_2 + k_3^2) R_{qh} - (k_1^2 \hat{k}_2 + \hat{k}_3^2) R_{dh} \\ & + \left(\frac{k_1 k_4 (1 - k_2)}{1 - k_1^2 - k_3 k_4} - \frac{k_1 \hat{k}_4 (1 - \hat{k}_2)}{1 - k_1^2 - \hat{k}_3 \hat{k}_4} \right) \omega_h \hat{L}_{dh} \end{aligned} \tag{35}$$

where R_{dh}^{err} is the estimation error, and

$$\hat{k}_2 = \frac{\hat{L}_{dh}}{\hat{L}_{qh}}, \ \hat{k}_3 = \frac{L_{dq}}{\hat{L}_{qh}}, \ \hat{k}_4 = \frac{L_{dq}}{\hat{L}_{dh}} \tag{36}$$

From the analysis of (22) and (33), the third term on the right side of (35) is negligible, thus the estimation error is dependant on the difference between d-axis and q-axis HF resistances. For the test machine, R_{dh} is assumed to be equal to R_{qh}. The estimation of HF resistance is summarized as in Algorithm 1.

D. Inverter Nonlinearity and PM Flux Variation Discussion

1) Influence of Inverter Nonlinearity: According to [28], [29], the voltage distortion due to inverter nonlinearity is

$$u_x^{err} = u_{xf}^{err} + u_{xh}^{err} \approx \text{sign}(i_{xf}) U_0 + R_{xh}^{vsi}(i_{xf}) i_{xh} \tag{37}$$

where the subscript x denotes the phase (phase a, phase b or phase c), that is, $x = a$, b or c; u_x^{err} denotes the inverter distorted voltage error on phase x; U_0 is saturation voltage of the inverter; R_x^{vsi} is the inverter equivalent HF resistance that is a nonlinear function of the phase fundamental current i_x^f; i_x^f and i_x^h are the fundamental and HF current components of phase x; the subscript '$_f$' means it is fundamental component, and '$_h$' means it is HF component. Here, the inverter equivalent HF resistance can be approximated as in (38) [25], where k is a model parameter depending only on the inverter.

$$R_{xh}^{vsi} = \frac{2 U_0 \cdot k \cdot e^{-k i_{xf}}}{(1 + e^{-k i_{xf}})^2} \tag{38}$$

From (37), the inverter nonlinearity will cause distortions to both the fundamental and HF voltages. This paper considers the HF resistance, thus only the HF voltage distortion is of interest. By applying Park transformation to the HF voltage distortions in abc-axis ($[u_{ah}^{err}, u_{bh}^{err}, u_{ch}^{err}]^T$), the inverter distorted HF voltage error in d-axis can be obtained as in (39) [25].

$$u_{dh}^{err} = \tfrac{2}{3} i_{dh} \left(R_{ah}^{vsi} \cos^2 \theta + R_{bh}^{vsi} \cos^2 (\theta_b) + R_{ch}^{vsi} \cos^2 (\theta_c) \right) \tag{39}$$

where $\theta_b = \theta - 2\pi/3$ and $\theta_c = \theta + 2\pi/3$. Therefore, the inverter equivalent HF resistance in d-axis is

$$R_{dh}^{vsi} = \tfrac{2}{3}\left(R_{ah}^{vsi}\cos^2\theta + R_{bh}^{vsi}\cos^2(\theta_b) + R_{ch}^{vsi}\cos^2(\theta_c)\right) \tag{40}$$

Therefore, the actual HF voltage applied to the d-axis is

$$u_{dh}^{act} = u_{dh} - u_{dh}^{err} \tag{41}$$

Thus, the HF resistance considering inverter nonlinearity is

$$\hat{R}_{dh}^{act} = \mathrm{Re}\left(\frac{u_{dh} - u_{dh}^{err}}{i_{dh}}\right) = \hat{R}_{dh} - R_{dh}^{vsi} \tag{42}$$

where $Re(Z)$ is a function taking the real part of Z. The investigations in [14], [25], [28], [29] show that the inverter equivalent HF resistance is almost zero when the phase fundamental current is larger than 1 A. Therefore, if all the three phase currents are larger than 1 A, we have

$$\texttt{If} \quad i_{af},\, i_{bf},\, i_{cf} > 1, \quad \texttt{Then} \quad R_{dh}^{vsi} \approx 0 \tag{43}$$

Above analysis demonstrates that if the measurements are obtained when the stator current is much larger than 1 A, the inverter nonlinearity is negligible during the estimation.

2) Influence of PM Flux Variation due to Temperature Rise: It is known that the PM flux decreases linearly as the PM temperature increases [32], [33]. However, the HF model (8) demonstrates that the variation of PM flux due to temperature rise will have an impact on the fundamental components but not on the HF component as the term related to PM flux has been cancelled in the HF model. Hence, the PM flux variation will not affect the impedance estimation. On the other hand, the temperature rise will result in the decrease of the PM flux as well as the increase of HF resistance. Therefore, both the PM flux and the HF resistance can be explored for PM temperature estimation. This paper focuses on PM temperature estimation using the HF resistance and improves the estimation performance by considering the cross-coupling effect.

IV. Implementation of HF Resistance and PM Temperature Estimation

Fig. 1 presents the control diagram for HF resistance and PM temperature estimation with HF voltage injection. In the control diagram, the HF voltage signal is superimposed on the reference voltage and fed to the PMSM through a voltage source inverter. The injected voltage will induce an HF current signal. In general, the switching frequency should be ten or more times larger than the bandwidth of the current controller in order to ensure the performance of current control. In most motor drive systems, the switching frequency is usually higher than 5 kHz (the switching frequency is set to be 10 kHz in the test system), which is sufficient to generate the required signal for temperature estimation. A band stop filter (BSF) is employed in the current feedback loop to filter out the HF current component. This aims to avoid the interaction between the HF component and the PI controller so that the current control will not be affected. The BSF filter utilized is a second-order filter, whose

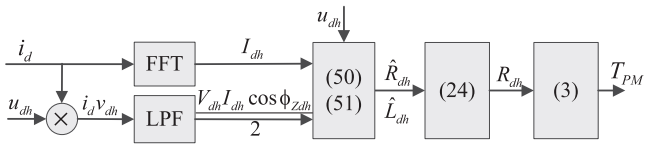

Fig. 2. The diagram of HF resistance and PM temperature estimation.

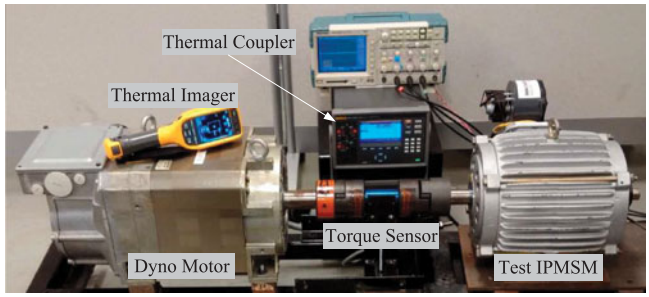

Fig. 3. The experimental setups for PM temperature estimation.

transfer function is

$$H(s) = \frac{s^2 + \omega_n^2}{s^2 + 2\xi\omega_n s + \omega_n^2} \tag{44}$$

where s is the Laplace operator, ω_n is the natural frequency, ξ is the damping ratio. The parameters of the BSF used are as follows: the natural frequency is selected to be the same as the injected signal and the damping ratio related to the filter quality factor is selected to be 0.707.

Fig. 2 presents the diagram of the HF resistance and PM temperature estimation. The inputs are the HF voltage u_{dh} and d-axis current i_d. At first, a FFT is applied to i_d to get the magnitude of the HF current component I_{dh}. In order to extract the phase angle ϕ_{Zdh}, (the phase difference between v_{dh} and i_{dh}), from the current measurement, the current i_d is multiplied by u_{dh} and then a low pass filter (LPF) is applied to $u_{dh} i_d$ as shown in Fig. 2. The d-axis current can be expanded in the Fourier series as

$$i_d = I_{d0} + \sum_i I_{di}\cos(\omega_i t - \phi_i) \tag{45}$$

where I_{d0} is the DC component and the second term on the right of (45) contains the harmonic components including the one in (12) with $\omega_i = \omega_h$. When i_d is multiplied by u_{dh}, it is

$$u_{dh} i_d = V_{dh}\left(I_{d0} + \sum_{i\neq h} I_{di}\cos(\omega_i t - \phi_i)\right)\cos(\omega_h t)$$
$$+ 0.5 V_{dh} I_{dh}\cos(2\omega_h t - \phi_{Zdh}) + 0.5 V_{dh} I_{dh}\cos(\phi_{Zdh}) \tag{46}$$

As can been seen from (46), only the last term is the DC component, and other terms are the HF components. Thus, the LPF is able to filter out the HF components, and the DC component can be obtained after the LPF. In other words, when a LPF is applied to $u_{dh} i_d$, the result is

$$\mathrm{LPF}\,(u_{dh} i_d) = 0.5 V_{dh} I_h \cos(\phi_{Zdh}) \tag{47}$$

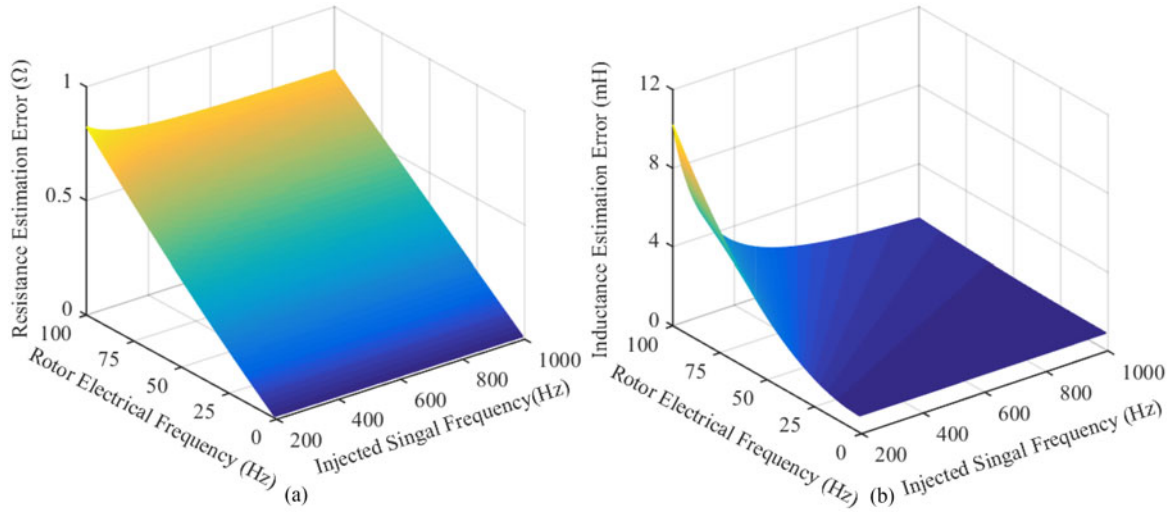

Fig. 4. Estimation error with respect to rotor speed and signal frequency. (a) HF resistance estimation error. (b) Inductance estimation error.

In this way, the phase angle can be obtained from

$$\cos\phi_{Zdh} = \frac{2\text{LPF}\left(u_{dh}i_d\right)}{V_{dh}I_h} \tag{48}$$

The LPF used is a second-order LPF. The transfer function is

$$H(s) = \frac{\omega_n^2}{s^2 + 2\xi\omega_n s + \omega_n^2} \tag{49}$$

Thus, (15) and (16) can be updated as

$$\hat{R}_{dh} = 2\text{LPF}\left(u_{dh}i_d\right)/I_{dh}^2 \tag{50}$$

$$\omega_h\hat{L}_{dh} = \sqrt{(V_{dh}/I_{dh})^2 - \hat{R}_{dh}^2} \tag{51}$$

After these steps, the HF resistance and PM temperature can be calculated from (24) and (3), respectively.

The extraction of the HF components from the measurements should be conducted during the steady state as the performance could be affected during the transient state. Hence, the proposed estimation should be conducted during the steady state in order to ensure better estimation performance. On the other hand, the temperature variation has a very large time constant, thus it is unnecessary to perform temperature estimation at every sampling time. Instead, the temperature estimation can be performed at a predefined interval (e.g., every 1 or 2 minutes). If the machine is under a transient state, the proposed temperature estimation should be postponed to the time when the machine reaches the steady state.

V. Experimental Investigations

A. Experimental Setup

The proposed PM temperature estimation approach is evaluated on a laboratory designed PMSM drive system as shown in Fig. 3, which is prototyped for direct-drive EV applications. The detailed finite element analysis (FEA) design parameters of the test machine are listed in Table I. In the test machine, the thermal detectors have been installed in the windings during machine prototyping, which can measure the winding temperature to calculate the accurate winding resistance. Moreover, during machine prototyping, some small windows are intentionally left on the test machine as can be seen from Fig. 3. Through these windows, we are able to see the magnets and thus able to measure the PM temperature by using the thermal imager. In the drive system, the test machine is controlled by FPGA-based real-time simulator and fed by an IGBT stack, while the dyno is controlled independently. The control diagram with $i_d = 0$ control strategy is employed for motor control as shown in Fig. 1 to simplify the implementation of the proposed temperature estimation method. However, the proposed approach is applicable to other control strategies as well. This is because the DC component of the d-axis current does not affect the extraction of the HF components for PM temperature estimation.

TABLE I
Finite Element Analysis Design Parameters of the Test PMSM

Rated power	4.25 kW	Unsaturated d-axis inductance	37.5 mH
Rated current	15 A	Unsaturated q-axis inductance	87.5 mH
Rated speed	575 rpm	PM flux	0.67 Wb
Resistance	1 Ω	Number of Poles	8

B. Numerical Results

Numerical studies on the test PMSM are performed to investigate how the cross-coupling effect affects the HF impedance estimation. Fig. 4 presents the HF impedance estimation error with respect to the rotor electrical speed ω and injected signal frequency ω_h. It can be seen that for a fixed ω_h, HF resistance estimation error increases as ω increases; while for a fixed ω, it is approximately constant for different ω_h. However, the inductance estimation error increases as ω increases and decreases as ω_h increases. Fig. 5 presents the HF impedance estimation error with respect to the mutual inductance, where L_{dq} varies from 0.5 mH to 5 mH but the rotor speed and the injected signal frequency are fixed to 10 and 200 Hz, respectively. It can be seen that both the resistance and inductance estimation errors increase linearly with the increase of L_{dq}. Thus, neglecting cross-coupling effect will cause great error to HF resistance estimation.

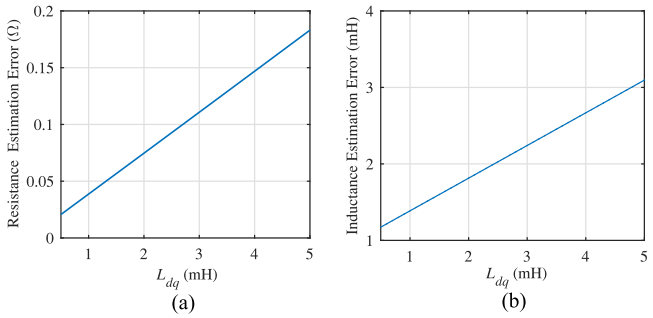

Fig. 5. Estimation error with respect to the mutual inductance. (a) HF resistance estimation error. (b) Inductance estimation error.

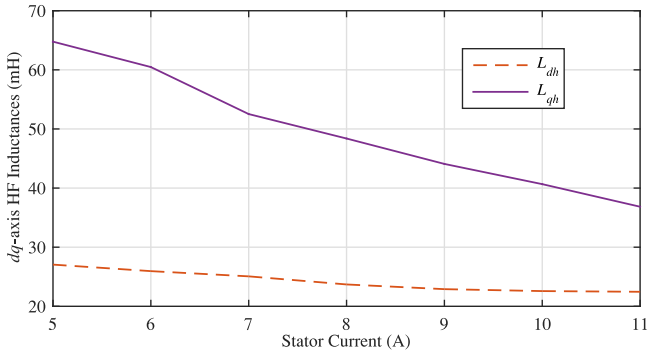

Fig. 6. The estimated dq-axis HF inductances of the test PMSM.

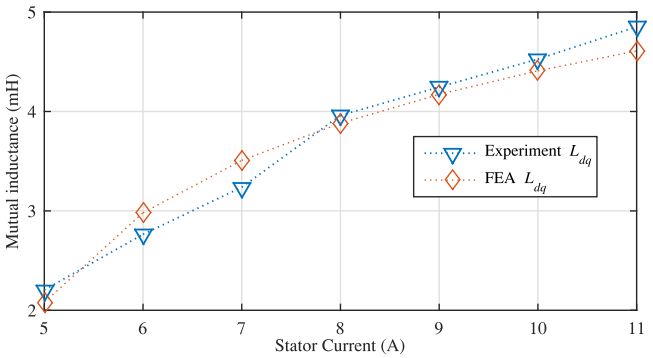

Fig. 7. The estimated mutual inductance of the test PMSM.

The estimated dq-axis HF inductances of the test PMSM are shown in Fig. 6, which shows that the dq-axis HF inductances decrease as the stator current increases. Thus, the magnetic saturation has a great effect on the dq-axis inductances and thus the dq-axis inductances should be estimated by using the proposed equations. Fig. 7 shows the estimated mutual inductance of the test PMSM and the one from FEA at different stator currents. It can be seen that the mutual inductance is increasing with the increase of the stator current. Thus, the cross-coupling effect is getting more severe with the increase of stator current. Hence, considering the cross-coupling effect will improve the estimation performance.

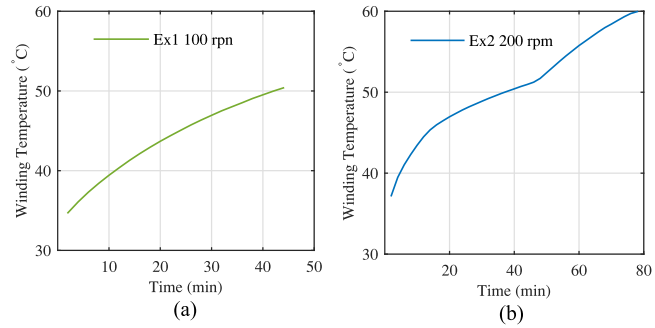

Fig. 8. Measured winding temperature. (a) First test. (b) Second test.

C. Experimental Results

When the test machine reaches the steady state, the HF voltage is added to the d-axis voltage reference to induce the HF current response. According to existing investigations [18], [19], [26], the frequency of the injected signal is selected to be about 150 $\sim$ 200 Hz larger than the operating frequency of the test machine and the magnitude should be around 3% of the DC bus voltage to ensure that the induced adverse effects are negligible. Hence, the frequency is selected to be 200 Hz and its magnitude is selected to be 15 V in the tests. In order to perform temperature estimation, the current measurements are sampled, the magnitude and phase angle of the HF current response are extracted, and the PM temperature is estimated by using the proposed equations.

Two tests are conducted to evaluate the proposed PM temperature estimation approach under different speeds. In both tests, the test machine is operating under rated current and the output torque is about 60 Nm. This is because operating under rated current can help to induce a quick rise of PM temperature. In the first test, the motor operates at 100 rpm and 200 rpm for the second test. The reason of selecting these two test conditions is that at low speeds we can monitor PM temperature by using the thermal imager, which can be used to evaluate the estimation performance of the proposed approach. However, at high speeds it becomes challenging to measure the PM temperature due to the high rotating speed of the rotor, thus it will be explored in the future work. On the other hand, as demonstrated by the analysis in Fig. 4, the error due to cross-coupling effect increases as motor speed increases. The experiments are conducted at low speed to demonstrate that the proposed approach can improve the estimation performance even at low speed conditions. During the experiment, the HF voltage signal is continuously injected for HF resistance and PM temperature estimation. The temperature variation has a large time constant, thus the temperature increases or decreases at a very slow speed. Hence, the HF resistance and PM temperature estimation is conducted every 2 minutes during the experiment. Similarly, the winding temperature is detected by the thermocouples every 2 minutes. In order to validate PM temperature estimation, the thermal imager is used to manually measure the surface PM temperature through the window on the test machine.

Fig. 8(a) presents the winding temperature during the first test, which is measured by the installed thermocouples. At the

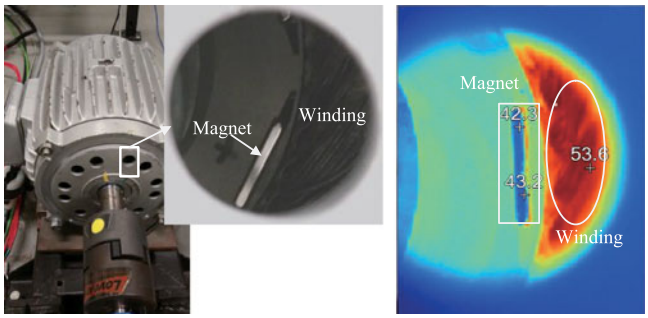

Fig. 9. PM temperature measured by the thermal imager.

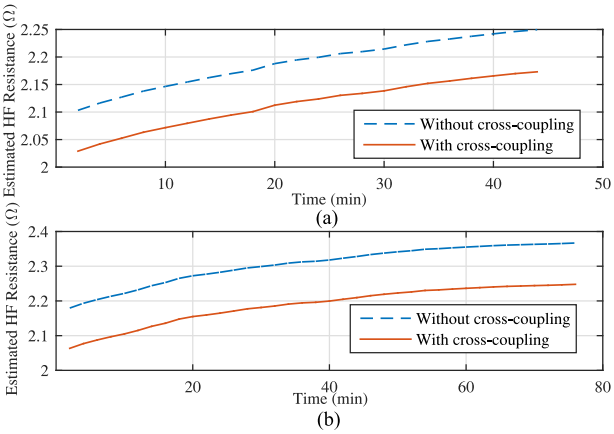

Fig. 10. The estimated HF resistances with and without considering the cross-coupling effect. (a) First test. (b) Second test.

beginning, the winding temperature is 35 °C, and it increases to 50 °C at the end. The thermal image obtained from the thermal imager is shown in Fig. 9. Both the winding temperature and the PM temperatures can be obtained from the thermal image. As can be seen from Fig. 9, the winding temperature is higher than the magnet temperature due to the dominant stator winding copper losses. Moreover, the temperature on the PM is not evenly distributed, and the temperature at the center is lower than that at the boundary, but the difference between temperatures on different points are not significant. The thermal image can indicate the surface temperature of the PM, which is not exactly the same as the inside PM temperature. The average value of the temperature measured from the thermal imager will be regarded as the true temperature to evaluate the proposed estimation approach.

After the measurements are collected, the HF resistance can be estimated by using Algorithm 1. Fig. 10(a) presents the estimated HF resistance with and without considering the cross-coupling effect. It can be seen that without considering the cross-coupling effect, the estimated HF resistance is 2.10 Ω at 30 °C and 2.25 Ω at 50 °C, while considering it, the estimated HF resistance is 2.03 Ω at 30 °C and 2.17 Ω at 50 °C. As can be seen from (18), the estimation error caused by cross-coupling effect is mainly depending on $k_1 k_4 (1 - k_2)\omega_h L_{dh} = (1 - k_2)\omega L_{dq} \approx 0.08\ \Omega$. Hence, at a specific condition, the estimation error due to cross-coupling effect is constant, which is proportional to mutual inductance.

Using the estimated HF resistance, the estimated PM temperature with and without considering the cross-coupling effect is

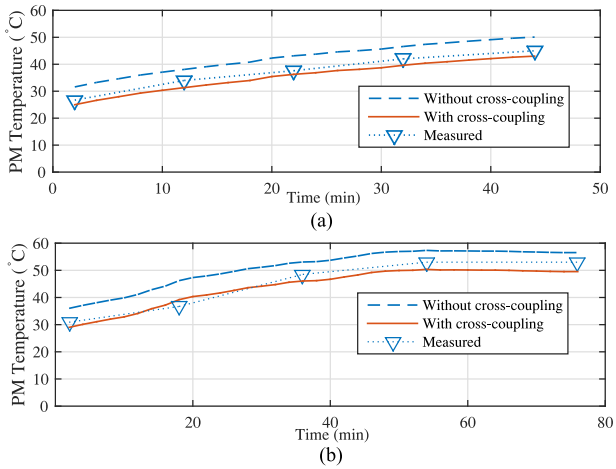

Fig. 11. The estimated PM temperature with and without considering the cross-coupling effect. (a) First test. (b) Second test.

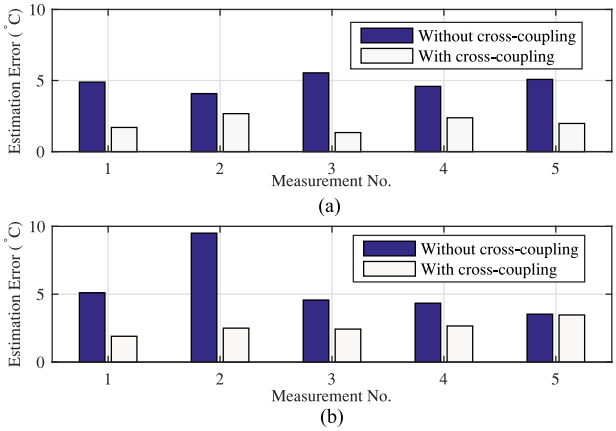

Fig. 12. The estimation error with and without considering the cross-coupling effect. (a) First test. (b) Second test.

shown in Fig. 11(a). The PM temperature is estimated from the thermal model of the HF resistance, so the estimated temperature could be regarded as the average temperature of the PMs. It can be seen that without considering the cross-coupling effect, the estimated PM temperature is 31 °C at the beginning and 50 °C at the end, while considering it the estimated PM temperature is 25 °C at the beginning and 43 °C at the end. Moreover, the PM surface temperature is about 27 °C at the beginning and 45 °C at the end. The estimation error with respect to the measured PM temperature is shown in Fig. 12(a). It can be seen that without considering the cross-coupling effect, the estimation error is 4 °C at the beginning and 6 °C at the end, while considering it, the estimation error is 2 °C at the beginning and 2 °C at the end. The maximum estimation error considering cross-coupling effect is about 4 °C, while that without considering it is about 6 °C. Thus, the estimation error without considering the cross-coupling effect is larger than the proposed approach. Therefore, the proposed approach has improved the PM temperature estimation performance by considering the cross-coupling effect.

During the second experiment, the winding temperature increases from about 35 to 60 °C as shown in Fig. 8(b), while The PM temperature increases from 31 to 53 °C as can be seen from

Fig. 11(b). The estimated HF resistances are shown in Fig. 10(b) and the estimated PM temperatures are shown in Fig. 11(b). The estimation error with respect to the measured PM temperature is shown in Fig. 12(b). It can be seen that without considering the cross-coupling effect, the estimation error is 5 °C at the beginning and 3.5 °C at the end; while the estimation of the proposed approach is 2 °C at the beginning and 3.5 °C at the end. Thus, the proposed approach is able to improve the PM temperature estimation accuracy by considering the cross-coupling effect.

VI. Conclusion

The HF voltage injection based PM temperature estimation has been improved in this paper by considering the cross-coupling effect, which is validated with experimental results. The proposed approach involves the inductances, which can vary during machine operation due to magnetic saturation. Thus, it is necessary to build a look-up-table of inductances for online PM temperature estimation, which will not only reduce the influence on the machine drive, but also simplify the implementation. The injected HF signal for temperature estimation will inevitably induce additional machine losses. This paper employs a continuous signal injection for demonstration, which can also induce more temperature rise. However, the HF signal is not necessary to be continuously injected in practical applications as the temperature variation has a very large time constant. Hence, it can be injected at a predefined interval to perform temperature estimation. Moreover, in order to ensure the impact on the machine drive to be negligible, the magnitude of the HF signal is usually selected to be around 3% of the DC bus voltage. In such a way, the impact on the global efficiency could be negligible in practical applications.

Appendix: Proof to (18) and (19)

Based on (17), (52) can be obtained. Since $\omega_h^2 L_{qh}^2 >> R_{qh}^2$, (52) can be simplified as (53). Based on (53), (18) and (19) can be directly obtained.

$$\begin{aligned}\hat{Z}_{dh} &= R_{dh} + j\omega_h L_{dh} + \frac{(\omega L_{dh} + j\omega_h L_{qd})(\omega L_{qh} - j\omega_h L_{dq})}{R_{qh} + j\omega_h L_{qh}} \\ &= R_{dh} + j\omega_h L_{dh} \\ &\quad + \frac{(k_1 L_{dh} + jL_{qd})(k_1 L_{qh} - jL_{dq})(R_{qh} - j\omega_h L_{qh})}{R_{qh}^2/\omega_h^2 + L_{qh}^2}\end{aligned} \tag{52}$$

$$\begin{aligned}\hat{Z}_{dh} &= R_{dh} + j\omega_h L_{dh} \\ &\quad + \frac{(k_1 L_{dh} + jL_{qd})(k_1 L_{qh} - jL_{dq})(R_{qh} - j\omega_h L_{qh})}{L_{qh}^2} \\ &= R_{dh} + j\omega_h L_{dh} + (k_1^2 k_2 + k_3^2 + jk_1 k_3(1 - k_2)) \\ &\quad \times (R_{qh} - j\omega_h L_{qh}) \\ &= R_{dh} + j\omega_h L_{dh} + (k_1^2 k_2 + k_3^2) R_{qh} + k_1 k_4 (1 - k_2)\omega_h L_{dh} \\ &\quad + j((-k_1^2 - k_3 k_4)\omega_h L_{dh} + k_1 k_3 (1 - k_2) R_{qh})\end{aligned} \tag{53}$$

References

[1] J. Zhang, H. Yao, and G. Rizzoni, "Fault diagnosis for electric drive systems of electrified vehicles based on structural analysis," *IEEE Trans. Veh. Technol.*, vol. 66, no. 2, pp. 1027–1039, Feb. 2017.

[2] F. Betin *et al.*, "Trends in electrical machines control: Samples for classical, sensorless, and fault-tolerant techniques," *IEEE Ind. Electron. Mag.*, vol. 8, no. 2, pp. 43–55, Jun. 2014.

[3] V. Ruuskanen, J. Nerg, J. Pyrhnen, S. Ruotsalainen, and R. Kennel, "Drive cycle analysis of a permanent-magnet traction motor based on magneto-static finite-element analysis," *IEEE Trans. Veh. Technol.*, vol. 64, no. 3, pp. 1249–1254, Mar. 2015.

[4] J. O. Estima and A. J. Marques Cardoso , "Efficiency analysis of drive train topologies applied to electric/hybrid vehicles," *IEEE Trans. Veh. Technol.*, vol. 61, no. 3, pp. 1021–1031, Mar. 2012.

[5] J. Wang, X. Yuan, and K. Atallah, "Design optimization of a surface-mounted permanent-magnet motor with concentrated windings for electric vehicle applications," *IEEE Trans. Veh. Technol.*, vol. 62, no. 3, pp. 1053–1064, Mar. 2013.

[6] K. Liu, Z. Zhu, and D. Stone, "Parameter estimation for condition monitoring of PMSM stator winding and rotor permanent magnets," *IEEE Trans. Ind. Electron.*, vol. 60, no. 12, pp. 5902–5913, Dec. 2013.

[7] Y. S. Lin, K. W. Hu, T. H. Yeh, and C. M. Liaw, "An electric-vehicle IPMSM drive with interleaved front-end dc/dc converter," *IEEE Trans. Veh. Technol.*, vol. 65, no. 6, pp. 4493–4504, Jun. 2016.

[8] A. Specht, O. Wallscheid, and J. Bocker, "Determination of rotor temperature for an interior permanent magnet synchronous machine using a precise flux observer," in *Proc. Int. Conf. Power Electron.*, May 2014, pp. 1501–1507.

[9] B. O. Wallscheid and J. Bcker, "Global identification of a low-order lumped-parameter thermal network for permanent magnet synchronous motors," *IEEE Trans. Energy Convers.*, vol. 31, no. 1, pp. 354–365, Mar. 2016.

[10] D. Diaz Reigosa, D. Fernandez, Z.-Q. Zhu, and F. Briz, "PMSM magnetization state estimation based on stator-reflected pm resistance using high-frequency signal injection," *IEEE Trans. Ind. Appl.*, vol. 51, no. 5, pp. 3800–3810, Sep. 2015.

[11] K. Liu and Z. Zhu, "Online estimation of the rotor flux linkage and voltage-source inverter nonlinearity in permanent magnet synchronous machine drives," *IEEE Trans. Power Electron.*, vol. 29, no. 1, pp. 418–427, Jan. 2014.

[12] K. Liu, Z. Zhu, Q. Zhang, and J. Zhang, "Influence of nonideal voltage measurement on parameter estimation in permanent-magnet synchronous machines," *IEEE Trans. Ind. Electron.*, vol. 59, no. 6, pp. 2438–2447, Jun. 2012.

[13] K. Liu and Z. Zhu, "Position-offset-based parameter estimation using the adaline nn for condition monitoring of permanent-magnet synchronous machines," *IEEE Trans. Ind. Electron.*, vol. 62, no. 4, pp. 2372–2383, Apr. 2015.

[14] J. Guerrero, M. Leetmaa, F. Briz, A. Zamarron, and R. Lorenz, "Inverter nonlinearity effects in high-frequency signal-injection-based sensorless control methods," *IEEE Trans. Ind. Appl.*, vol. 41, no. 2, pp. 618–626, Mar. 2005.

[15] M. Seilmeier and B. Piepenbreier, "Sensorless control of PMSM for the whole speed range using two-degree-of-freedom current control and HF test current injection for low-speed range," *IEEE Trans. Power Electron.*, vol. 30, no. 8, pp. 4394–4403, Aug. 2015.

[16] Q. Tang, A. Shen, X. Luo, and J. Xu, "PMSM sensorless control by injecting HF pulsating carrier signal into ABC frame," *IEEE Trans. Power Electron.*, vol. 32, no. 5, pp. 3767–3776, May 2017, doi: 10.1109/TPEL.2016.2583787.

[17] G. Feng, C. Lai, and N. Kar, "Expectation maximization particle filter and Kalman filter based permanent magnet temperature estimation for PMSM condition monitoring using high-frequency signal injection," *IEEE Trans. Ind. Informat.*, vol. 13, no. 3, pp. 1261–1270, Jun. 2017.

[18] D. Reigosa, F. Briz, P. Garcia, J. Guerrero, and M. Degner, "Magnet temperature estimation in surface pm machines using high-frequency signal injection," *IEEE Trans. Ind. Appl.*, vol. 46, no. 4, pp. 1468–1475, Jul. 2010.

[19] D. Diaz Reigosa, D. Fernandez, H. Yoshida, T. Kato, and F. Briz, "Permanent-magnet temperature estimation in PMSMS using pulsating high-frequency current injection," *IEEE Trans. Ind. Appl.*, vol. 51, no. 4, pp. 3159–3168, Jul. 2015.

[20] M. Seilmeier, S. Ebersberger, and B. Piepenbreier, "HF test current injection-based self-sensing control of PMSM for low- and zero-speed range using two-degree-of-freedom current control," *IEEE Trans. Ind. Appl.*, vol. 51, no. 3, pp. 2268–2278, May 2015.

[21] Z. Zhu and L. Gong, "Investigation of effectiveness of sensorless operation in carrier-signal-injection-based sensorless-control methods," *IEEE Trans. Ind. Electron.*, vol. 58, no. 8, pp. 3431–3439, Aug. 2011.
[22] B. Stumberger, G. Stumberger, D. Dolinar, A. Hamler, and M. Trlep, "Evaluation of saturation and cross-magnetization effects in interior permanent-magnet synchronous motor," *IEEE Trans. Ind. Appl.*, vol. 39, no. 5, pp. 1264–1271, Sep. 2003.
[23] Y. Li, Z. Zhu, D. Howe, C. Bingham, and D. Stone, "Improved rotor-position estimation by signal injection in brushless ac motors, accounting for cross-coupling magnetic saturation," *IEEE Trans. Ind. Appl.*, vol. 45, no. 5, pp. 1843–1850, Sep. 2009.
[24] Y. Li, Z. Zhu, D. Howe, and C. Bingham, "Modeling of cross-coupling magnetic saturation in signal-injection-based sensorless control of permanent-magnet brushless ac motors," *IEEE Trans. Magn.*, vol. 43, no. 6, pp. 2552–2554, Jun. 2007.
[25] G. Wang *et al.*, "Self-commissioning of permanent magnet synchronous machine drives at standstill considering inverter nonlinearities," *IEEE Trans. Power Electron.*, vol. 29, no. 12, pp. 6615–6627, Dec. 2014.
[26] D. Reigosa, D. Fernandez, T. Tanimoto, T. Kato, and F. Briz," Comparative analysis of BEMF and pulsating high frequency current injection methods for PM temperature estimation in PMSMs," *IEEE Trans. Power Electron.*, vol. 32, no. 5, pp. 3691–3699, May 2017.
[27] G. Luo, R. Zhang, Z. Chen, W. Tu, S. Zhang, and R. Kennel, "A novel nonlinear modeling method for permanent-magnet synchronous motors," *IEEE Trans. Ind. Electron.*, vol. 63, no. 10, pp. 6490–6498, Oct. 2016.
[28] L. M. Gong and Z. Q. Zhu, "A novel method for compensating inverter nonlinearity effects in carrier signal injection-based sensorless control from positive-sequence carrier current distortion," *IEEE Trans. Ind. Appl.*, vol. 47, no. 3, pp. 1283–1292, May 2011.
[29] Y. Park and S. K. Sul, "A novel method utilizing trapezoidal voltage to compensate for inverter nonlinearity," *IEEE Trans. Power Electron.*, vol. 27, no. 12, pp. 4837–4846, Dec. 2012.
[30] S. Mahdavi and K. Hameyer, "High frequency equivalent circuit model of the stator winding in electrical machines," in *Proc. XXth Int. Conf. Electr. Mach.*, Marseille, 2012, pp. 1706–1711.
[31] N. Z. Popov, S. N. Vukosavic, and E. Levi, "Motor temperature monitoring based on impedance estimation at PWM frequencies," *IEEE Trans. Energy Convers.*, vol. 29, no. 1, pp. 215–223, Mar. 2014.
[32] M. T. Thompson, "Practical issues in the use of NdFeB permanent magnets in maglev, motors, bearings, and eddy current brakes," *Proc. IEEE*, vol. 97, no. 11, pp. 1758–1767, Nov. 2009.
[33] S. Li, B. Sarlioglu, S. Jurkovic, N. Patel, and P. Savagian, "Comparative analysis of torque compensation control algorithms of interior permanent magnet machines for automotive applications considering the effects of temperature variation," *IEEE Trans. Transp. Electrific.*, vol. 3, no. 3, pp. 668–681, Sep. 2017.

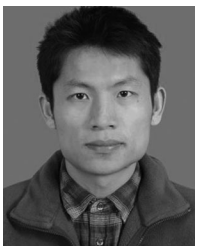

Guodong Feng (M'15) received the B.S. and Ph.D. degrees in engineering from the School of Information, Science and Technology, Sun Yat-sen University, Guangzhou, China, in 2010 and 2015, respectively. From 2013 to 2015, he also worked as a Research Assistant with the Sun Yat-sen University and Carnegie Mellon University Shunde International Joint Research Institute, Shunde, China. He is currently a Postdoctoral Fellow with the Department of Electrical and Computer Engineering, University of Windsor, Windsor, ON, Canada. His research interests include advanced signal processing, optimization and electrical machine design, control, and testing.

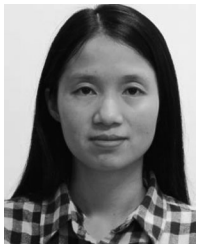

Chunyan Lai (M'17) received the B.S. degree in engineering from the Sun Yat-sen University, Guangzhou, China, in 2010, and the Ph.D. degree in electrical and computer engineering from the University of Windsor, Windsor, ON, Canada, in 2017. Between 2010 and 2013, she spent two and a half years in the industry in China. She is currently a Postdoctoral Fellow under the Canada Research Chair Program in electrified transportation systems with the Department of Electrical and Computer Engineering, University of Windsor. Her research interests include electric machines, drives and other power electronic related applications.

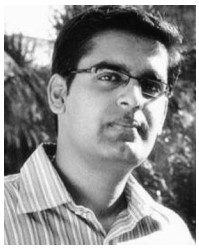

K. Lakshmi V. Iyer (M'16) received the B.Tech. degree in electronics and communication engineering from SASTRA University, Thanjavur, India, in 2009, and the M.A.Sc. and Ph.D. degrees in electrical and computer engineering from the University of Windsor, Windsor, ON, Canada, in 2011 and 2016, respectively. He is currently a Research Scientist and Industry Liaison Officer under the Canada Research Chair Program in electrified transportation systems with the University of Windsor, Canada. His research interests include electric motor and drives and associated sustainable energy solutions for electrified transportation applications.

Narayan C. Kar (SM'07) received the B.Sc. degree in electrical engineering from the Bangladesh University of Engineering and Technology, Dhaka, Bangladesh, in 1992, and the M.Sc. and Ph.D. degrees in electrical engineering from the Kitami Institute of Technology, Hokkaido, Japan, in 1997 and 2000, respectively. He is a Professor with the Department of Electrical and Computer Engineering, the University of Windsor, Windsor, ON, Canada, where he holds the Canada Research Chair position in electrified transportation systems. His current research interests include analysis, design, and control of electrical machines for electrified vehicle applications.